ESAIM: PROCEEDINGS AND SURVEYS, October 2024, Vol. 77, p. 267-284
Emmanuel Franck, Hélène Hivert, Guillaume Latu, Hélène Leman, Bertrand Maury, Michel Mehrenberger, Laurent Navoret

A WELL-BALANCED SCHEME USING EXACT SOLUTIONS TO THE TWO SPECIES VLASOV-POISSON SYSTEM

Nicolas Crouseilles [1], Mohammed Lemou [2], Guillaume Morel [3] and Pierre Navaro [4]

Abstract. In this work, we consider the numerical approximation of the two-species Vlasov-Poisson system using Eulerian methods. A family of exact non homogeneous stationary solutions are constructed using elliptic functions. Then, speci c numerical schemes are proposed to compute solutions which remain close to a given stationary solution since standard schemes fail to capture such a dynamics on coarse meshes. The strategy is based on a suitable decomposition of the solution (in the spirit of f approaches) which can be easily combined with any classical Vlasov solvers. For unstable dynamics, a projection technique is proposed in order to dynamically change the equilibrium. Finally, numerical tests are proposed to illustrate the good behavior of the proposed strategy.

1. Introduction

The system considered in this work is the two species Vlasov-Poisson system which is a simple model used to describe a collisionless plasma in one dimension in space and velocity. It reads

$$\begin{cases} \partial f^+ + v\partial f^+ - \partial \partial_v f^+ = 0; \\ \partial f^- + v\partial f^- + \partial_x \partial_v f^- = 0; \end{cases} \tag{1}$$

where the potential := (t; x) satis es the Poisson equation

$$\partial_x = \int_R (f - f^+)dv; \tag{2}$$

where > 0 is the mass ratio, $f^+ := f^+(t; x; v)$ and f := f (t; x; v) denote the distribution functions for the ions and electrons respectively, depending on time 0, space x and velocity v. The system (1) is supplemented with initial conditions

$$f^+(0; x; v) = f^+_{in}(x; v); \qquad f^-(0; x; v) = f^-_{in}(x; v);$$

on the domain x 2 [0; L], v 2 R where we assume periodic boundary conditions in x and vanishing boundary conditions in v.

[1] Univ Rennes, Inria (Mingus team), IRMAR UMR 6625 and ENS Rennes, France.
[2] Univ Rennes, CNRS, IRMAR UMR 6625, France.
[3] IMT Atlantique, France.
[4] Univ Rennes, CNRS, Inria (Mingus team), IRMAR UMR 6625, France.

Article published online by EDP Sciences and available at https://www.esaim-proc.org or https://doi.org/10.1051/proc/202477267

Since the dynamics of the Vlasov-Poisson system may be very complicated, we will essentially focus in this work on initial conditions which are a perturbation of a given non homogeneous equilibrium. Note the large time analysis of the Vlasov-Poisson system around non homogeneous equilibrium is a very active domain (see [8, 9]). From a numerical perspective, the dynamics is quite challenging to capture since various behaviors may happen (stability, unstability, lamentations, vortices, : : :). Even if high order numerical schemes are required, standard schemes may fail to capture such behaviors on coarse meshes and lead to unphysical instabilities. The goal of this work is therefore to construct numerical schemes which improve the quality of the numerical solution when the initial functions is chosen to be a perturbation of non homogeneous equilibrium. Let us note that in many physical applications, the initial condition of Vlasov type models is taken as a perturbation of an equilibrium (see [12, 18, 19]...). Restricting ourselves to this con guration, it is natural to design well-balanced numerical schemes by using a suitable decomposition of the unknown, where the one part corresponds to the equilibrium and the other part corresponds to the out of equilibrium part. This kind of micro-macro decomposition has been introduced to derive asymptotic-preserving schemes [6, 20] but also to design well-balanced schemes in the presence of collisions [10, 25], but also recently in the collisionless case [11, 19, 24] to improve the accuracy of a Vlasov solver. Let us also mention [13, 14] in the context of collisional radiative transfer equation. In this latter case, the approach bears similarities with the so-called f approach [3] developed for Particle-In-Cell methods.

In our case, we will consider the following decomposition of the solution $f = f_0 + g$ where f_0 is a given equilibrium and g can be seen as a perturbation of f_0, even if g can be large when the dynamics drives the solution far from the equilibrium f_0. The unknown of the reformulated problem will thus be the perturbation g. Then, the main motivation from this strategy is to design a numerical scheme for the reformulated problem which

(i) preserves *exactly* the equilibrium f_0,
(ii) is able to capture the correct behavior of the solution (in some representative cases) for large time even when coarse meshes are considered.

However, it is well known that computing analytically non homogeneous stationary states of (1)-(2) is not that easy. In practice, periodic non homogeneous stationary states are usually considered numerically, and the procedure can be quite tedious [11,12] since it involves a nonlinear elliptic equation to solve. In this work we will construct a family of exact stationary non homogeneous solutions to the system (1)-(2) (in one dimension in space and velocity). As a function of $v^2/2$ (x), these solutions belong to the so-called BGK waves [2] whose stability have been widely studied in the past decades whether analytically [15, 16, 21, 22] or numerically [7, 12, 26]. However, to our knowledge, exact non-homogeneous periodic BGK solutions have not yet been derived.

In summary, we propose a micro-macro decomposition based numerical scheme to explore the dynamics of (1)-(2) when the initial condition is a periodic perturbation of such an analytic stationary state. As we shall see, this decomposition has a strong links with the so-called f method [3] and can be combined with all classical numerical methods for Vlasov type models. Note that in this work, high order Eulerian methods will be used. The numerical tests we have conducted show good behavior compared to standard method when coarse meshes are considered.

The outlines of the paper is the following. In Section 2 we show how to derived exact periodic non homogeneous stationary solutions to (1)-(2) using Jacobi elliptic functions. Then in Section 3, we present the derivation of the well-balanced scheme. Finally, in Section 4, several numerical results are shown to illustrate the good behavior of the proposed scheme.

2. Stationary solutions

2.1. Main idea

In this section we construct exact solutions to the system (1)-(2). To present the main idea we search for stationary solutions to (1)-(2) under the following form

$$\begin{cases} f^+(x,v) = \sqrt{(-a)}\left(r_1 e^{2a(\frac{v^2}{2}+\phi(x))} + \frac{r_2}{2} e^{a(\frac{v^2}{2}+\phi(x))}\right), \\ f^-(x,v) = \sqrt{(-a)}\left(s_1 e^{2a(\frac{v^2}{2\mu}-\phi(x))} + \frac{s_2}{2} e^{a(\frac{v^2}{2\mu}-\phi(x))}\right), \end{cases} \tag{3}$$

with $a, r_1, s_1, r_2, s_2 \in \mathbb{R}$, $a < 0$ (let recall that μ is the mass ratio). Since $f^\pm$ are functions of $\frac{v^2}{2}+\phi$, they belong to the so-called BGK waves [2] and it is possible to show that such functions are solutions to (1) simply by inserting (3) in (1). The difficult part is to determine, if it exists, the potential associated with $f^\pm$ through (2). Usually, this is done numerically [11, 12] by solving a nonlinear elliptic problem. In the following, we shall give some exact solutions and show that the potential associated with the solutions (3) can be expressed using Jacobi elliptic functions.

The construction of our solutions is based on the following equality

$$ae^{2a\phi}\partial_x\phi = e^{a\phi}\partial_x(e^{a\phi}) - (\partial e^{a\phi})^2. \tag{4}$$

To determine ϕ we proceed as follow. First we insert (3) in (2) to obtain

$$\partial_x\phi = s_1 e^{-2a\phi} + s_2 e^{-a\phi} - r_2 e^{a\phi} - r_1 e^{2a\phi}. \tag{5}$$

Now, multiplying this equality by $ae^{2a\phi}$ and using (4) enable to get

$$e^{a\phi}\partial_x(e^{a\phi}) - (\partial e^{a\phi})^2 = a(s_1 + s_2 e^{a\phi} - r_2 e^{3a\phi} - r_1 e^{4a\phi}).$$

Finally, the change of variable $u := e^{a\phi}$ leads to

$$u\partial_x u - (\partial u)^2 = a(s_1 + s_2 u - r_2 u^3 - r_1 u^4). \tag{6}$$

Therefore, if we find some solutions to (6), we obtain solutions to the Vlasov-Poisson equation (1). Note however that since we are interested in real solutions one must have $a < 0$, moreover for the solutions to be physically relevant we need $f^\pm \geq 0$ for all $x, v \in \mathbb{R}$ in (3).

Remark 2.1. *It is also possible to multiply* (5) *by* $ae^{-a\phi}$ *and make the change of variable* $v = e^{-a\phi}$. *In this case, one obtains the following equation (instead of* (6)*)*

$$v\partial_x v - (\partial v)^2 = -a(s_1 v^4 + s_2 v^3 - r_2 v - r_1). \tag{7}$$

If $\mu = 1$, *this is simply equivalent to exchange* f^+ *and* f^-.

2.2. Some solutions to (1)-(2)

The solutions constructed in this section are based on a general function w which satisfied the following non linear differential equation

$$(\partial w)^2 = \alpha w^4 + \beta w^3 + \gamma w^2 + \delta w + \varepsilon. \tag{8}$$

It is well known that solutions to (8) can be constructed using elliptic functions [1, 4, 27, 29]. For example, if we consider the simple case of the Jacobi elliptic functions (see Appendix A), then (8) is satisfied with $\beta = \delta = 0$ and some $\alpha, \gamma, \varepsilon \in \mathbb{R}$. However, using directly such functions to solve (6) only leads to solutions which are not physical. To obtain positive real solutions, one must change these

functions with a suitable transformation. Here we simply add a constant $b \in \mathbb{R}$ and consider instead the functions $w + b$ but more general transformations such as linear fractional transformation of the form $(cw + b)/(ew + d)$ could also be considered.

Lemma 2.2. *Let w satisfies (8). Then the function $z := w + b$ satisfies the following equality*

$$z\partial_{xx} z - (\partial_x z)^2 = -b^4 + b^3 - b^2 + b + (2b^3 - \frac{3b^2}{2} + b)z + (-2b + \frac{1}{2})z^3 + z^4 \quad (9)$$

Proof. Since $\partial_x(\partial_x w)^2 = 2\partial_x w \partial_{xx} w$, one can deduced from (8) the equation satisfied by $(\partial_x w)^2$ and $\partial_{xx} w$. The rest of the proof is straightforward using the equality $w = z - b$ and rearranging the terms. □

Consider a function z defined as in Lemma 2.2. As mentioned in Remark 2.1 we have two kinds of solutions.

(1) The first solution is obtained with the change of variable $u = e^a$. Matching (6) and (9) one gets

$$r_1 = \frac{1}{a}; \; r_2 = \frac{+4b}{2a}; \; s_1 = \frac{-b^4 + b^3 - b^2 + b}{a}; \; s_2 = \frac{4b^3 - 3b^2 + 2b}{2a}; \quad (10)$$

and the potential reads

$$\alpha(x) = \frac{1}{a}\log(w + b); \quad (11)$$

(2) The second solution is obtained with the change of variable $v = e^{-a}$. Matching (7) and (9) gives

$$r_1 = \frac{-b^4 + b^3 - b^2 + b}{a}; \; r_2 = \frac{4b^3 - 3b^2 + 2b}{2a}; \; s_1 = \frac{-1}{a}; \; s_2 = \frac{+4b}{2a}: \quad (12)$$

and the potential reads

$$\alpha(x) = -\frac{1}{a}\log(w + b): \quad (13)$$

Now we give some examples for the solutions. The following solutions are based on some Jacobi elliptic functions which satisfy the non linear ordinary differential equation (27) and where the coefficients are given in the Table 1. Note however that since we consider here functions under the form $cf(\omega x; k)$, (27) must be rescaled accordingly. In the following the coefficients α; β; γ; δ and the function w are given explicitly together with a positivity condition. The solutions (3) can then be deduced using the relations (10)-(11) or (12)-(13).

Solution 1. The function considered is $w = c\,\mathrm{dn}(\omega(x - x_0); k)$. For this function one has

$$\alpha = \frac{\omega^2}{c^2}; \quad \beta = 0; \quad \gamma = -\omega^2(2 - k^2); \quad \delta = 0; \quad \eta = -\omega^2(1 - k^2)c^2: \quad (14)$$

and a sufficient condition to obtain positivity is

$$c > 0; \quad b \geq -(1 + \sqrt{2})c; \quad 1 \geq k \geq 0:$$

Solution 2. The function considered is $w = c\,\mathrm{nd}(\omega(x - x_0); k)$. For this function one has

$$\alpha = \frac{\omega^2(k^2 - 1)}{c^2}; \quad \beta = 0; \quad \gamma = -\omega^2(2 - k^2); \quad \delta = 0; \quad \eta = -\omega^2(c^2): \quad (15)$$

and a sufficient condition to obtain positivity is

$$c > 0; \quad b > -(1 + \sqrt{2})c; \quad \sqrt{1 - \frac{(3 + 2\sqrt{2})c^2}{b^2}} \geq k \geq 0:$$

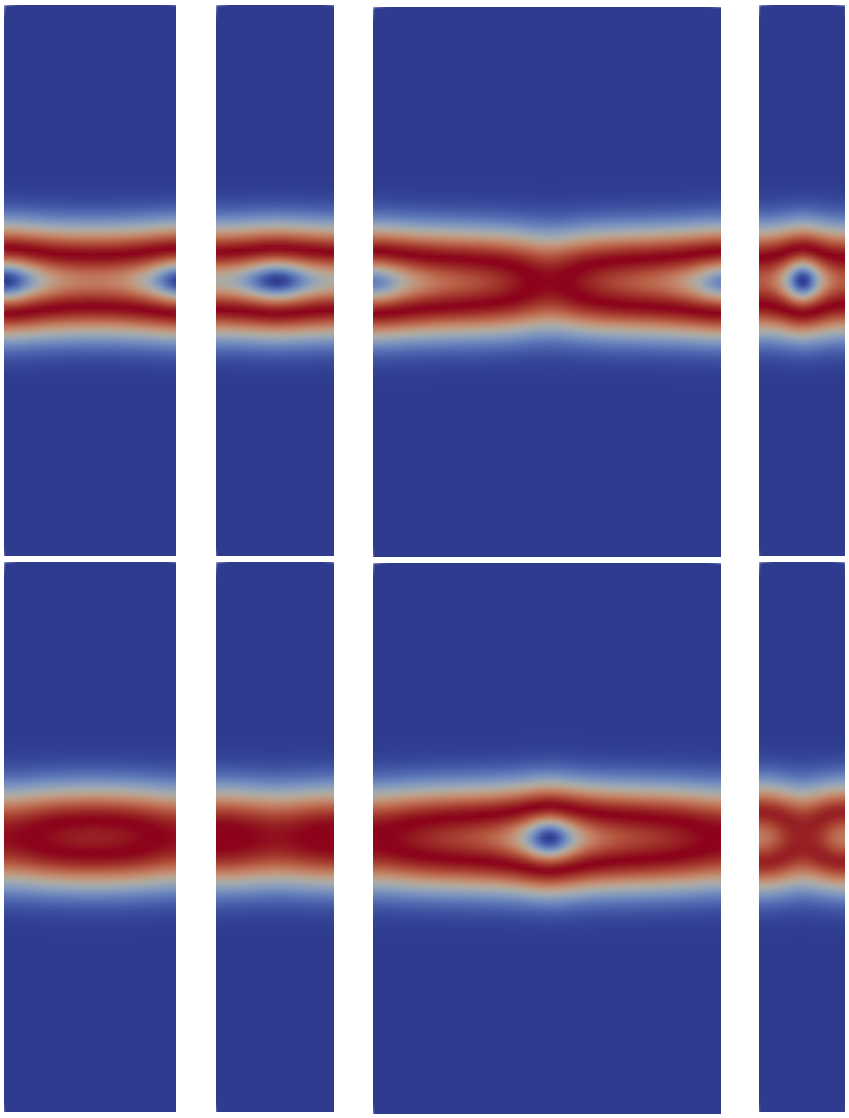

FIGURE 1. Some graphical illustrations of solutions 1 to 4 (from left to right) over one spatial period. First line: $f_0^+(x;v)$. Second line: $f_0(x;v)$.

Solution 3. The function considered is $w = c\,cn(\ (x \quad x_0);k)$. For this function one has

$$= \frac{k^2\ ^2}{c^2}; \qquad = 0; \qquad = {}^2(2k^2 \quad 1); \qquad = 0; \qquad = {}^2(1 \quad k^2)c^2:$$

and a sufficient condition to obtain positivity is

$$c > 0; \quad b > \frac{(1+\sqrt{2}+\sqrt{7+4\sqrt{2}})c}{2}; \quad 1 \quad k \quad \sqrt{\frac{((\ 2+\sqrt{2})b \quad 2c)c^2}{2(b \quad c)(b+c)(b \quad \sqrt{2}b+c)}}:$$

The last example is based on the Weierstrass elliptic function $\wp(x;g_2;g_3)$ which satisfies the nonlinear ordinary differential equation (28).

Solution 4. The function considered is $w = \frac{c}{\wp(x - x_0; g_2; g_3)}$. For this function one has

$$= \frac{g_3^{\ 2}}{c^2}; \quad = \frac{g_2^{\ 2}}{c}; \quad = 0; \quad = 4c^{\ 2}; \quad = 0:$$

To have a simple positivity condition we take $g_2 = 0$. And a sufficient condition to obtain positivity is then

$$c > 0; \quad b > 0; \quad g_2 = 0; \quad g_3 \quad \frac{4(7 + 5\sqrt{2})c^3}{b^3}:$$

On Figure 1, some graphical illustrations of these 4 solutions are given with the following coefficients

solution 1: $b = 1 + \sqrt{2}$, $k^2 = 0:97$,
solution 2: $b = 2(1 + \sqrt{2})$, $k^2 = 0:75$,
solution 3: $b = 3$, $k^2 = 0:97$,
solution 4: $b = (4(7 + 5\sqrt{2}))^{1=3}$, $g_2 = 0$, $g_3 = 1$, $k^2 = 0:9$,

and for all the solutions $a = \ 1$, $c = 1$, $= 1$, $x_0 = 0$.

Note that the spatial periods are not the same for each solution. Indeed, solutions 1 and 2 are related to the elliptic functions dn and nd which have spatial periods $2K(k)$ (where $K(k)$ can be defined as an elliptic integral see Appendix A). Since solutions 1 and 2 have different values for k, they also have different spatial periods (see Figure 1). Solution 3 is related to the elliptic function cn and has period $4K(k)$ while solution 4 is related to the Weierstrass elliptic function and has a spatial period which is also different from the three previous solutions.

Remark 2.3. *Note that some parameters can be used to control the stability of the stationary solutions. By stability, we mean that a perturbation of the stationary solution leads to a solution which moves away the stationary solution with a certain rate. If the rate is smaller, the solution is said to be "more stable". For example increasing* b *or decreasing* a *(while the other coefficients are fixed) makes the solution more stable. Similarly, increasing* k *makes the solution more stable. Some examples are given in Figures 2 in which the time evolution of* (23) *is plotted for different values of* k *and* b *(the initial solution is chosen as a perturbation of amplitude* $10^{\ 3}$ *of the equilibrium, similarly as in* (25)*). On the left part of Figure 2, one can observe that when* k *increases, the solution remains close to the equilibrium (*$k^2 = 0:99$*, purple curve) whereas for* $k = 0:9$ *(red curve), the solution moves quickly away from the equilibrium. Similarly on the right part of Figure 2, the largest value of* b *(*$b = 1:2 + \sqrt{2}$*, purple curve) leads to stable results whereas the smallest value of* b *(*$b = 1 + \sqrt{2}$*, red curve) leads to unstable results. Of course, more investigations would be welcome but the stability of non homogeneous stationary solutions is known to be a challenging problem that is not the main goal of this work and we restrict ourselves to some numerical illustrations.*

Remark 2.4 (Periodic and hyperbolic solutions). *Solutions 1 to 3 are periodic for* $0 \quad k < 1$ *and hyperbolic when* $k = 1$ *since the Jacobi elliptic functions degenerate towards hyperbolic functions when* $k \ ! \ 1$ *(see Appendix A).*

3. A well-balanced scheme

In this section we show how to derive a well-balanced scheme for the system (1)-(2). More precisely we will focus in this section on a discretization of (1) based on a micro-macro decomposition [10, 11, 17, 20, 23, 25]. In the rest of this section, we will denote $_f$ the potential associated with $(f \quad f^+)$ according to

$$@_x \ _f = \int_R (f \quad f^+)dv: \qquad (16)$$

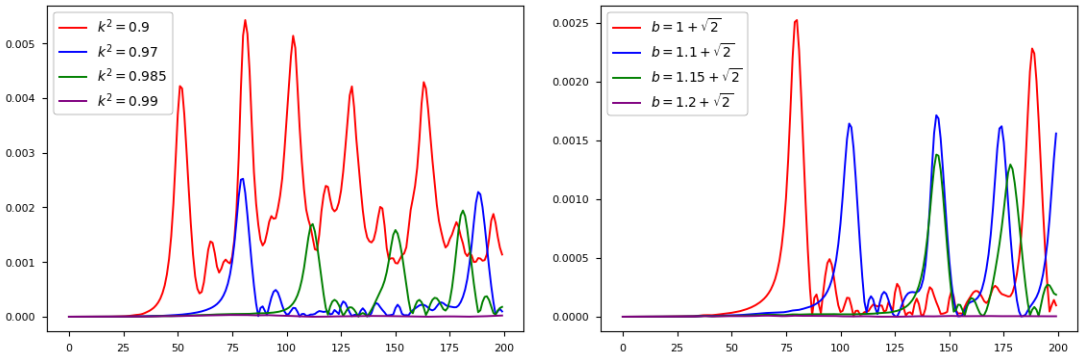

FIGURE 2. Left figure: time evolution of (23) for different values of k (the other parameters are $a = 1$; $= b = 1$; $m = k^2$; $x_0 = 0$) ; right figure: time evolution of (23) for different values of b (the other parameters are $a = 1$; $= 1$; $m = k^2 = 0.97$; $x_0 = 0$). For both figures, $L = 4K(k)$.

3.1. Preserving one stationary state

The main goal of this section is to design a numerical scheme which is able to preserve a given stationary state *exactly*. Indeed, it is known that standard schemes are not able to preserve a given stationary state due to numerical errors. Numerical schemes which are not well-balanced may produce spurious oscillations when approaching equilibria or near equilibrium solutions so that the numerical solution may become wrong. The well-balanced scheme presented in this section bears some similarities with the scheme introduced [11] for Vlasov-HMF and is able to preserve exactly one given stationary state to the system (1)-(2). To derive the scheme we perform the following decomposition

$$f(t;x;v) = f_0(x;v) + g(t;x;v); \tag{17}$$

where $f_0(x;v)$ does not depend on time and is a stationary solution to (1)-(2) associated with a potential $_{f_0}(x)$. Inserting (17) in (1) and using the notation $T = v@ @ @_v$, one gets

$$\begin{aligned} @g^+ + T_f(f_0^+ + g^+) &= 0; \\ @g + T_f(f_0 + g) &= 0: \end{aligned} \tag{18}$$

Moreover since f_0 is a stationary solution to (1)-(2) one has by definition $v@f_0^+ = @_{f_0}@f_0^+$ and $v@f_0 = @_x f_0@f_0$. Therefore, we get

$$\begin{aligned} T_f f_0^+ &:= (v@ @_f@)f_0^+; \\ &= (@_{f_0}@ @_f@)f_0^+; \\ &= (@_f @_{f_0})@f_0^+; \\ &= @_g@f_0^+; \end{aligned}$$

where $_g := _f - _{f_0}$ is the potential associated with g defined by $@_x {}_g = \int_R (g - g^+)dv$ according to (16). Similar calculations can be performed to get $T_f f_0 = @_x {}_g@f_0$ and finally (18) can reformulated as

$$\begin{aligned} @g^+ + T_f g^+ &= @_g@f_0^+; \\ @g + T_f g &= @_x {}_g@f_0: \end{aligned} \tag{19}$$

The potentials $_f$ and $_g$ satisfy the following Poisson equations

$$@_x\ _f = \int_R (f \quad f^+)dv; \quad @_x\ _g = \int_R (g \quad g^+)dv;$$

and the initial condition for g is given by

$$g^+(0;x;v) = f_{in}^+(x;v) \quad f_0^+(x;v); \quad g\ (0;x;v) = f_{in}(x;v) \quad f_0(x;v):$$

To solve numerically (19) we use a time splitting scheme where the term $@_x\ _g@_v f_0$ is treated as a source term. Equations (19) are then solved with three main steps (for simplicity we take $= 1$)

$$\begin{aligned} &(1) \quad @_t g = @_x\ _g@_v f_0; \\ &(2) \quad @_t g + v@_x g = 0; \\ &(3) \quad @_t g \quad @_x\ _f @_v g = 0: \end{aligned} \tag{20}$$

Integrated with respect to v the step (1) one observes that $\int_R g\ dv$ is constant and so is $_g$. Therefore, the step (1) can be solved exactly in time using an explicit Euler scheme since $\int_R g\ dv$ is constant along this stage. The steps (2) and (3) will be solved using semi-Lagrangian methods [5, 28] (for the interpolation, cubic B-spline are used [24]). In the numerical tests since the equilibrium will be obtained with the exact solutions derived in the previous section, the term $@_v f_0$ on the right hand side of (1) can be calculated analytically. It is also possible to calculate this term numerically provided that a high order method is used (for example a fourth order centered nite di erence approximation).

We consider the second order in time discretization given in [5] to solve (2) and (3) from t^n to t^{n+1}. In the following, t denotes the time step, g^n the semi-discretization in time of the unknown g at $t^n := n\ t$ and $g^{(k)}$ intermediate steps between t^n and t^{n+1}. For simplicity we drop the index but it is important to note that the steps of the procedure described below are computed at the same time for g^+ and g . This is required to solve (16) when evaluating $@_x\ _g$. One obtains the following algorithm

1: Solve step (1) of (20) over a half time step: $g^{(1)} = g^n + \frac{t}{2} @_x\ _{g^n} @_v f_0$ where $@_x\ _{g^n}$ is calculated with (16),

2: Solve step (2) of (20) over a half time step: $g^{(2)}(x;v) = g^{(1)}(x \quad v\frac{t}{2};v)$,

3: Update the value of $E^{(2)} := \quad @_x\ _{f^{(2)}}$ with (16) and $f^{(2)} := f_0 + g^{(2)}$;

4: Solve step (3) of (20) over a whole time step: $g^{(3)}(x;v) = g^{(2)}(x;v \quad E^{(2)}\ t)$,

5: Solve step (2) of (20) over a half time step: $g^{(4)}(x;v) = g^3(x \quad v\frac{t}{2};v)$.

6: Solve step (1) of (20) over a half time step: $g^{(5)} = g^{(4)} + \frac{t}{2} @_x\ _{g^{(4)}} @_v f_0$ where $@_x\ _{g^{(4)}}$ is calculated with (16),

(21)

Proposition 3.1 (Well-balanced scheme) *The scheme* (21) *is well-balanced for the stationary state* f_0.

Proof. It is enough to notice that if $f(0;x;v) = f_0(x;v)$ then $g(0;x;v) = 0$ and the splitting described previously preserves the zero solution exactly. □

3.2. Changing dynamically the equilibrium $f_0^{\pm}$

Even if the scheme described in Section 3.1 preserves one given stationary state, it is still possible to change this equilibrium during the simulation. Since we focus in this work on an initial condition which a perturbation of an equilibrium given in Section 2, it makes sense to consider these stationary states. This family of solutions depends on some parameters $a; b; c; ; x_0; k \in \mathbb{R}$ and is therefore of finite dimension. For example, one can minimize a given norm with respect to some of this parameters and consider for example

$$\min \left(\| f^{n;+} - f_{eq}^{+} \|_{L^2_{x,v}} + \| f^{n;} - f_{eq} \|_{L^2_{x,v}} \right); \tag{22}$$

where $f^{n;}$ denotes the numerical solution at time t^n and f_{eq} a family of exact solutions. The goal when minimizing (22) is to get the smallest perturbation g. The stationary state f_0 in the decomposition (17) can then be replaced with the new stationary state obtained when solving (22).

Ideally one would like to project on all the stationary states of the form $F(\frac{v^2}{2} - (x))$. However this seems complicated in practice, see for example [11, Section 3.6] for an attempt at the order 0.

In our case it is important to notice that nothing guarantees that the quality of the numerical solution is improved when minimizing (22). Therefore one has to choose the parameters of the optimization carefully. In the numerical tests we will simply consider a translation, that is minimizing with respect to x_0, which seems to be a reasonable choice for our examples.

Remark 3.2. *Here we have chosen to minimize the* $f^n - f_{eq}$ *to get a small perturbation* g *but other choices could be considered. For example one could try to minimize* $\partial_x f^n - \partial_x f_{eq}$ *and* $\partial_v f^n - \partial_v f_{eq}$ *to get a smoother perturbation* g.

4. Numerical results

In this section, the well-balanced scheme is tested and compared with a standard scheme for which the first step in (20) is simply omitted. More precisely the standard scheme consists simply in steps 2 to 5 of (21) which is a very classical discretization [5, 28]. The numerical tests will consist of an initial condition which is a perturbation of a given equilibrium. We shall study two different configurations

In the first one the solution stays close to the equilibrium. The numerical test is said to be stable.

For the second case the solution diverges from the equilibrium. The numerical test is said to be unstable.

To compare precisely the two schemes (classical and well-balanced), we will plot the following time dependent quantity

$$\left| \frac{\int_{[0;L]} \int_{\mathbb{R}} v^2 (f^{+}(t;x;v) - f_{eq}^{+}(x;v)) \, dx dv}{\int_{[0;L]} \int_{\mathbb{R}} v^2 f_{eq}^{+}(x;v) \, dx dv} \right|; \tag{23}$$

where f_{eq} is the initial equilibrium and we have arbitrarily chosen to represent the quantity (23) for f^{+}.

The space domain $[0; L]$ is discretized by a uniform grid of N_x points and periodic boundary conditions are considered. In all the numerical tests we will take $L = 4K(k)$ where $K(k)$ is the elliptic integral mentioned in Appendix A. In the velocity direction, we choose a truncated domain $[-10; 10]$ with a uniform grid of N_v points. Finally, $t^n = n\,\Delta t$, $n \in \mathbb{N}$ and $\Delta t > 0$ is the time step. For simplicity we will take $= 1$ in all the numerical tests. For the well-balanced scheme we choose initially $f_0 = f_{eq}$. The Julia version of the code is available on GitHub:
https://juliavlasov.github.io/VlasovPoissonTwoSpecies.jl/dev/simu/

4.1. A first stable numerical test

For this test we consider the initial equilibrium f_{eq} described by the second solution (15) with $= 1$, $a = -2$, $b = 2(1 + \sqrt{2})$, $c = 1$, $m = k^2 = 0.75$, $x_0 = 0$ and a final time $T = 200$. The initial function is

taken as the equilibrium with no perturbation

$$f(0,x,v) = f_{eq}(x,v). \tag{24}$$

We compare two different approaches

- The standard scheme on a 64×64 mesh and $t = 0.2$.
- The well-balanced scheme from Section 3.1 on a 64×64 mesh and $t = 0.2$.

The results are displayed on Figure 3. Since the initial condition is simply a stationary solution no reference solution is needed: the solution is supposed to stay at the equilibrium. It is well known that classical schemes have no difficulties to preserve homogeneous equilibriums ($E(x) = 0$). However, as illustrated by Figure 3, this is not the case anymore when non homogeneous equilibrium are considered. Indeed the Figure 3 shows that the well-balanced scheme capture exactly the stationary solution (24) at all times which is not the case for the standard scheme.

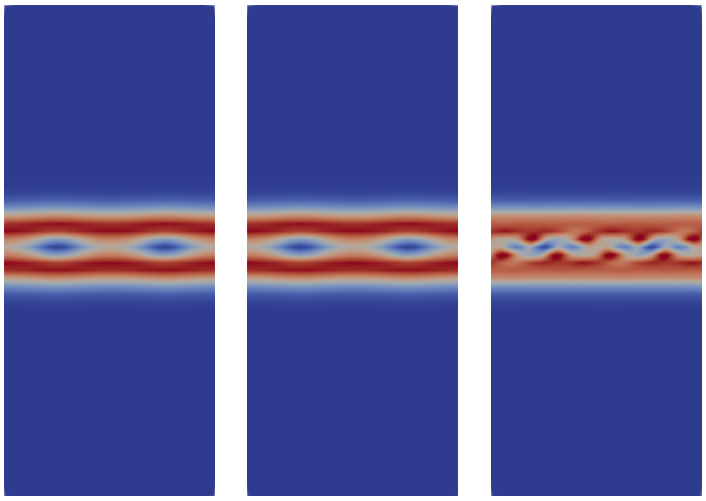

FIGURE 3. Phase space representation of the function f^+ for the first stable numerical test with no perturbation. From left to right: initial condition, well-balanced scheme at $T = 200$, standard scheme at $T = 200$.

4.2. A second stable numerical test

For this test we consider the initial equilibrium f_{eq} described by the first solution (14) with $= 1$, $a = -2$, $b = 1 + \sqrt{2}$, $c = 1$, $m = k^2 = 0.97$, $x_0 = 0$ and a final time $T = 200$. The initial function is chosen as a perturbation of the non homogeneous stationary solution f_{eq}

$$f(0,x,v) = f_{eq}(x,v)(1 + \varepsilon \cos(\frac{2\pi x}{4K(k)})), \tag{25}$$

with $\varepsilon = 0.001$ and we compare three different approaches

- The standard scheme on a 64×64 mesh and $t = 0.2$.
- The well-balanced scheme from Section 3.1 on a 64×64 mesh and $t = 0.2$.
- The reference solution is computed with the standard scheme on a 512×512 mesh and $t = 0.025$.

The results are displayed in Figure 4 where we plot the time history of the quantity defined in (23) for the three numerical methods. The well-balanced scheme correctly captures the reference solution (obtained by a refined mesh) which remains close to the stationary state while the solution obtained by the standard scheme on a coarse mesh is less accurate and leads to an (unphysical) unstable solution.

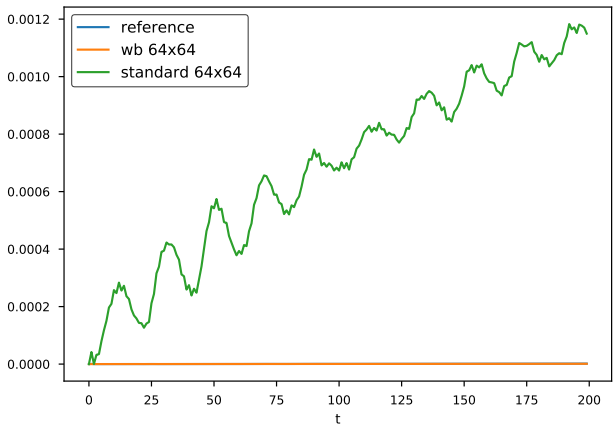

FIGURE 4. Second stable numerical test. Comparison between the well-balanced and standard scheme. Time history of the quantity (23). The well-balanced line overlapped the reference solution.

4.3. A first unstable numerical test

For this test we consider the initial equilibrium f_{eq} described by the first solution (14) with $= 1$, $a = -1$, $c = 1$, $m = k^2 = 0.97$, $x_0 = 0$ and a final time $T = 200$. The initial function is then written

$$f(0;x;v) = f_{eq}(x;v)(1 + " \cos(\frac{2x}{4K(k)} + 1)) ;$$

with $" = 0.001$. Note that, compare to the previous example, we have translated the perturbation, breaking the symmetry of the test and therefore making it unstable. As discussed in Remark 2.3, the parameter b has a strong influence on the stability rate of the test (see also Figure 2). Indeed, increasing the value of b from its smallest acceptable value ($b = 1 + \sqrt{2}$) makes the stationary solution more stable and as such, it delays the merging time of the two vortices involved in the initial condition (see Figures 5 and 7). Indeed, for $b = 1.12 + \sqrt{2}$, one can observe on Figure 5 that the two vortices get closer and closer before separating (first at time $t = 110$ and second at time $t = 130$) and finally merging at time $t = 200$. On the contrary, for smaller b like $b = 1 + \sqrt{2}$ (which will be the next numerical test), the merging time occurs at time $t = 75$ (see Figure 7). Note that when the two vortices interact, the quantity (23) presents peaks as illustrated in Figure 6 (three peaks can be observed, corresponding to three interactions).

We compare the following cases

- The standard scheme on a 64×64 mesh and $t = 0.2$.
- The standard scheme on a 128×128 mesh and $t = 0.1$.
- The well-balanced scheme from Section 3.1 on a 64×64 mesh and $t = 0.2$.
- The well-balanced scheme from Section 3.1 on a 64×64 mesh, $t = 0.2$ with a projection every 25 iterations as described in Section 3.2. For the norm chosen in the projection we arbitrarily choose the L^2 norm although other choices could be considered. The only parameter of the optimization is x_0.
- The reference solution is computed with the standard scheme on a 512×512 mesh and $t = 0.025$.

In Figure 6, we compare the quantity (23) for the cases described previously. Note that three main peaks appearing on the reference solution correspond to times where the holes interact, see Figure 5. Our goal is to approximate correctly these peaks illustrating that the dynamic of the solution is

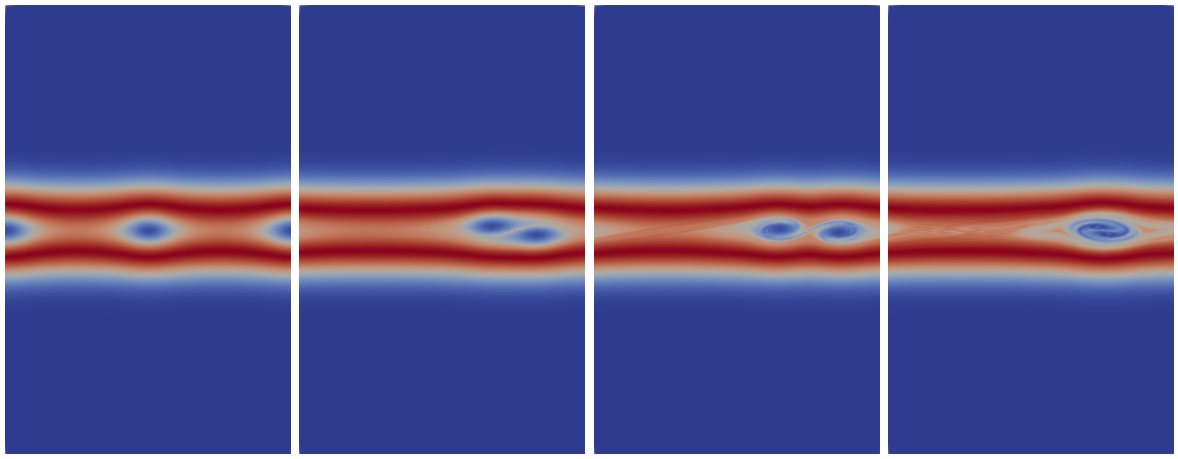

FIGURE 5. Phase space representation of the function f^+ at different times of the simulation for the test case 4.3 for $b = 1.12 + \sqrt{2}$. From left to right: $t = 0$, $t = 110$, $t = 130$ and $t = 199$. At the end of the simulation the holes initially on the center and on the right have merged.

correctly captured. If one looks on the left part of Figure 6, one can observe that the standard scheme completely fails to recover a correct approximation of the reference solution on a 64×64 mesh (actually the two holes do not even merge in this case). Considering a 128×128 mesh improves the numerical solution, however the times corresponding to the peaks are still wrong. On the contrary, the right part of Figure 6 shows that the well-balanced scheme is able to reproduce correctly the time of the first peak using a coarse mesh (64×64) both with and without projection technique. On this numerical test, the projection does not seem to improve a lot the quality of the numerical solution and it is therefore enough to consider the well-balanced scheme with the initial stationary state only.

4.4. A second unstable numerical test

For this second unstable numerical test, we take the same parameters as before except that $b = 1 + \sqrt{2}$. As mentioned before, since b is smaller, the solution will be more unstable compare to the previous case for which b was larger ($b = 1.12 + \sqrt{2}$). In particular, for this numerical test the holes interact and see each other but do not merge. For example, the second peak now represents a second time where two different holes interact, as illustrated in Figure 7. We compare the following cases

- The standard scheme on a 64×64 mesh and $t = 0.2$.
- The well-balanced scheme from Section 3.1 on a 64×64 mesh and $t = 0.2$.
- The well-balanced scheme from Section 3.1 on a 64×64 mesh, $t = 0.2$ with a projection every 25 iterations as described in Section 3.2. For the norm chosen in the projection we arbitrarily choose the L^2 norm although other choices could be considered. The only parameter of the optimization is x_0.
- The reference solution is computed with the standard scheme on a 512×512 mesh and $t = 0.025$.

The results are displayed on Figure 8 where the quantity (23) is given for the cases described previously. As noted before, the peaks which appear on Figure 8 show the times where the holes interact, see Figure 7 for more details. Once again, our goal is therefore to get a good approximation of the times when these peaks appear. On the left part of Figure 8, the standard and well-balanced schemes are compared. We can observe that the well-balanced scheme correctly captured the first peak which is not the case for the standard scheme. However, even if the first peak is correctly captured by the well-balanced scheme, the second peak is not well captured (for the the reference solution, it appears at time $t \simeq 130$ whereas for the well-balanced scheme, it appears later, around $t \simeq 185$). We

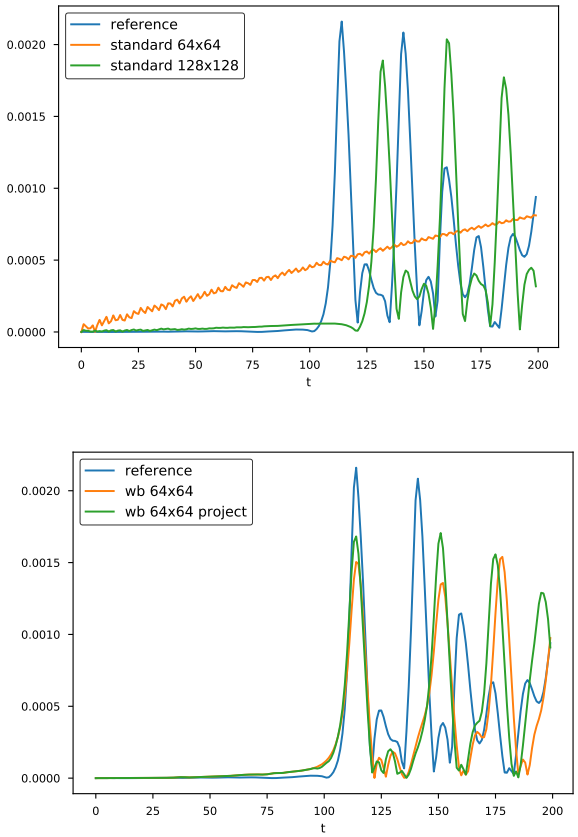

FIGURE 6. Time history of the quantity (23) for $b = 1.12 + \sqrt{2}$. Left: standard scheme on a 64×64 and 128×128 meshes. Right: well-balanced scheme on a 64×64 with and without a projection at $t = 115$ (until $t = 115$ the two schemes overlapped). The well-balanced scheme gives better results even on coarse meshes.

also consider on the right part of Figure 8 the well-balanced scheme with projection. We observe that the second peak obtains with the projection technique is closer to the reference solution.

5. Conclusion

In this work, the two-species Vlasov-Poisson system is studied. First, non homogeneous analytical stationary solutions are proposed using elliptic functions. Second, suitable numerical schemes are proposed to improve the numerical simulation of the dynamics around these equilibrium solutions compared to standard approaches. A first numerical scheme is able to capture exactly one given equilibrium by using a micro-macro type decomposition whereas in a second numerical scheme, the equilibrium associated to the decomposition is modified dynamically using an optimization step. Some numerical results illustrate the capabilities of the new approach on both stable and unstable configurations. In particular, the new methods are able to greatly improve the reliability of the numerical simulations when coarse phase space meshes are considered. Possible extensions using Particle-In-Cell methods might be interesting to investigate to reduce the noise, in the spirit of the δf method but in the non homogeneous case.

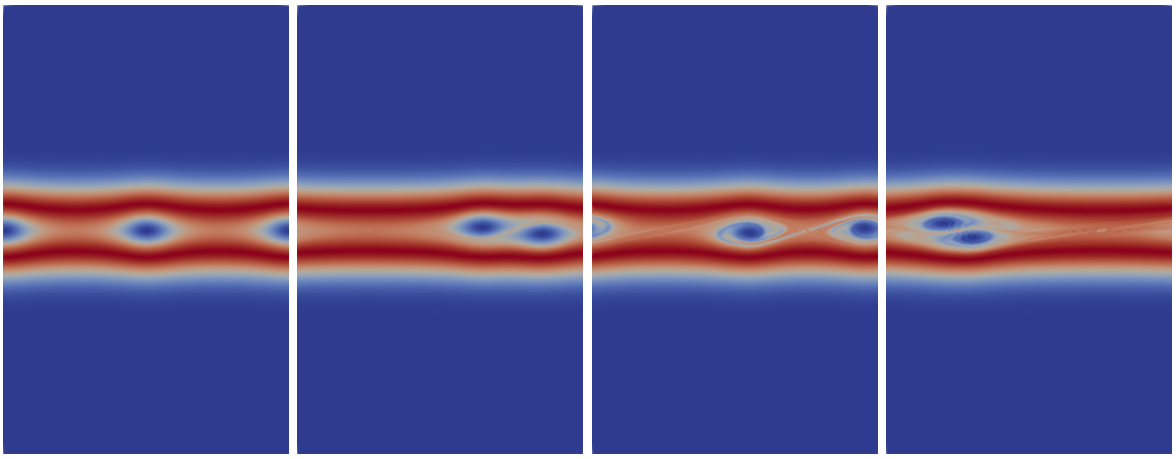

FIGURE 7. Phase space representation of the function f^+ at different times of the simulation for the test case 4.4 where $b = 1 + \sqrt{2}$. From left to right: $t = 0$, $t = 75$, $t = 100$ and $t = 130$. The holes interact but do not merge.

Aknowledgements

This project has been supported by the French Federation for Magnetic Fusion Studies (FR-FCM). This work has been carried out within the framework of the EUROfusion Consortium, funded by the European Union via the Euratom Research and Training Programme (Grant Agreement No 101052200 EUROfusion). Views and opinions expressed are however those of the author(s) only and do not necessarily reflect those of the European Union or the European Commission. Neither the European Union nor the European Commission can be held responsible for them. Finally, authors would like to thanks the CEMRACS organizers thanks to which this work has been completed.

A. Elliptic functions

In this appendix a very brief overview of the Jacobi elliptic functions and some of their main properties are given, for more details on elliptic functions see for example [1,4,27,29]. We adopt here the presentation from [27] and choose to introduce the Jacobi elliptic functions like the usual trigonometric functions replacing the unit circle with the (normalized) ellipse which satisfied the equation (see Figure 9)

$$(\frac{x}{a})^2 + y^2 = 1; \tag{26}$$

and define the modulus k as $k = \frac{\sqrt{a^2 - 1}}{a}$. For $k = 0$ (that is $a = 1$) we recover the equation of a circle and when $k \to 1$ (that is $a \to 1$) the ellipse became more and more stretched. Sometimes the notation $m := k^2$ is used.

The three main Jacobi elliptic functions are denoted $sn(u;k); cn(u;k); dn(u;k)$ can then be defined as follow

$$cn(u;k) = \frac{x}{a}; \quad sn(u;k) = y; \quad dn(u;k) = \frac{r}{a};$$

where the argument of the elliptic functions associated with a point P is defined as $u := \int_0^P r\,d\theta$, r is the (non constant) radius satisfying $x^2 + y^2 = r$ and $x = r\cos\theta$ and $y = r\sin\theta$ are the standard polar coordinates. The derivatives of the three main Jacobi elliptic functions satisfy

$$\frac{d}{du} sn = cn\,dn; \quad \frac{d}{du} cn = -sn\,dn; \quad \frac{d}{du} dn = -k^2\,sn\,cn:$$

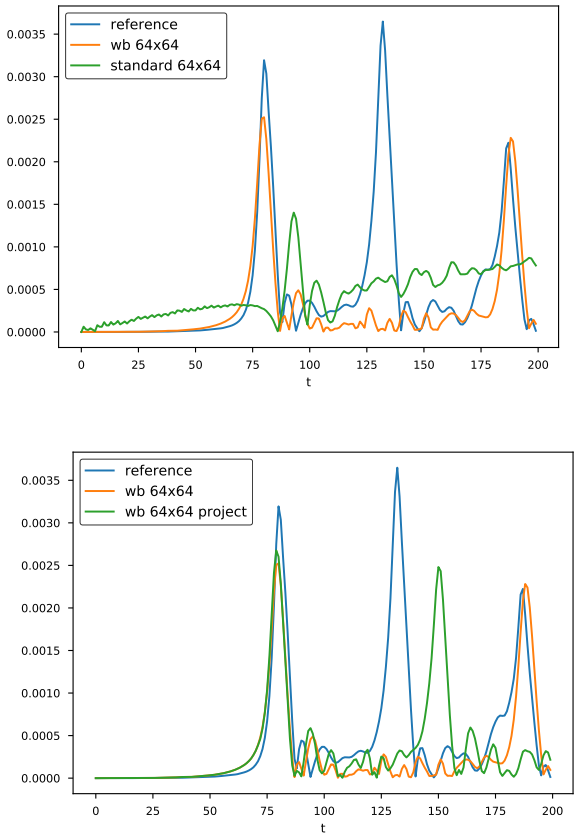

FIGURE 8. Time history of the quantity (23). Left: comparison of the standard scheme and the well-balanced scheme on a 64 64 mesh. Right: comparison of the well-balanced scheme with and without projection on a 64 64 mesh.

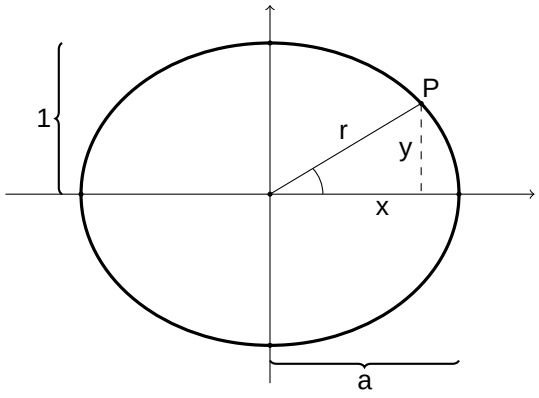

FIGURE 9. A representation of the ellipse given by equation (26).

For $k = 0$ one recovers the usual trigonometric functions associated to the circle and when $k \to 1$ the elliptic functions degenerate toward hyperbolic functions

$$\mathrm{sn}(u;0) = \sin u; \quad \mathrm{cn}(u;0) = \cos u; \quad \mathrm{dn}(u;0) = 1;$$

$$\mathrm{sn}(u;1) = \tanh u; \quad \mathrm{cn}(u;1) = \frac{1}{\cosh u}; \quad \mathrm{dn}(u;1) = \frac{1}{\cosh u}:$$

See Figure 10 for some graphical examples of the functions sn, cn and dn for different values of k. Other elliptic functions can also be defined as ratio of the three previous functions

$$\text{ns} := \frac{1}{\text{sn}}; \quad \text{nc} := \frac{1}{\text{cn}}; \quad \text{nd} := \frac{1}{\text{dn}}; \quad \text{cs} := \frac{\text{cn}}{\text{sn}}; \quad \text{ds} := \frac{\text{dn}}{\text{sn}}; \quad \text{sc} := \frac{\text{sn}}{\text{cn}}; \quad \text{dc} := \frac{\text{dn}}{\text{cn}}; \quad \text{sd} := \frac{\text{sn}}{\text{dn}}; \quad \text{cd} := \frac{\text{cn}}{\text{dn}};$$

Note that those functions are named by concatenation of the first letter from the numerator and denominator. These functions are periodic: the period of sn and cn is $4K$, and the period of dn is $2K$, where $K := K(k)$ is the value of u at the top of the ellipse where $(x; y) = (0; 1)$. The function $K(k)$ can also be defined from an elliptic integral. An important property of the Jacobi elliptic functions sn, cn and dn is that they satisfy the following nonlinear ordinary differential equation with respect to u

$$\left(\frac{d}{du}\text{sn}\right)^2 = (1 - \text{sn}^2)(1 - k^2\,\text{sn}^2);$$
$$\left(\frac{d}{du}\text{cn}\right)^2 = (1 - \text{cn}^2)(1 - k^2 + k^2\,\text{cn}^2);$$
$$\left(\frac{d}{du}\text{dn}\right)^2 = (\text{dn}^2 - 1)(1 - k^2 - \text{dn}^2).$$

More generally, all the Jacobi elliptic functions satisfy a nonlinear ordinary differential equation of the general form

$$\left(\frac{d}{dx}y\right)^2 := \alpha y^4 + \beta y^2 + \gamma; \tag{27}$$

where the coefficients α, β and γ are given in the Table 1. This kind of equations has various physical applications: they arise, for example, when studying solitons or the motion of a pendulum.

Finally we mention the Weierstrass function $\wp$ which is another kind of elliptic function. The function $\wp$ is different but related to the Jacobi elliptic functions. In particular, it satisfies the following nonlinear ordinary differential equation

$$\wp(z; g_2; g_3)'^2 = 4\wp(z; g_2; g_3)^3 - g_2\wp(z; g_2; g_3) - g_3; \tag{28}$$

where g_2, g_3 are called invariant. The Weierstrass function can be defined from the Jacobi elliptic functions. For more details see [4, 29].

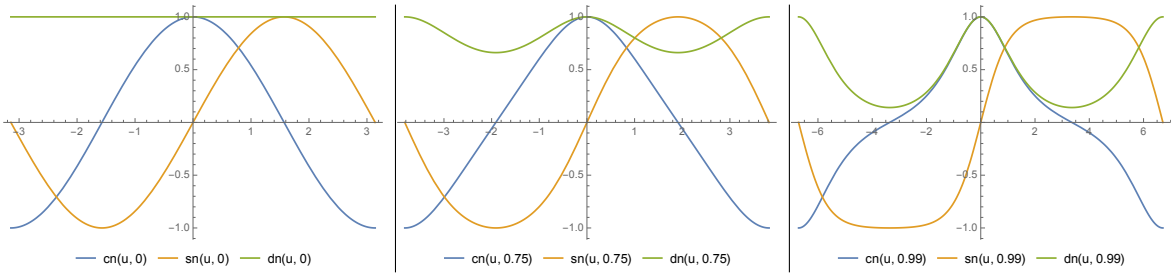

FIGURE 10. Representation of the three main Jacobi elliptic functions for different values of k. From left to right: $k = 0$, $k = 0.75$, $k = 0.99$.

References

[1] J. V. Armitage and W. F. Eberlein, *Elliptic Functions*, London Mathematical Society Student Texts, Cambridge University Press, 2006, doi:10.1017/CBO9780511617867.

[2] I. B. Bernstein, J. M. Greene, and M. D. Kruskal, *Exact nonlinear plasma oscillations*, Phys. Rev., 108 (1957), pp. 546 550, doi:10.1103/PhysRev.108.546, https://link.aps.org/doi/10.1103/PhysRev.108.546.

[3] S. Brunner, E. Valeo, and J. A. Krommes, *Collisional delta-f scheme with evolving background for transport time scale simulations*, Physics of Plasmas, 6 (1999), pp. 4504 4521, doi:10.1063/1.873738, https://doi.org/10.1063/1.873738, arXiv:https://doi.org/10.1063/1.873738.

sn	k^2	$1\quad k^2$	1
cn	k^2	$1+2k^2$	$1\quad k^2$
dn	1	$2\quad k^2$	$1+k^2$
ns	1	$1\quad k^2$	k^2
nc	$1\quad k^2$	$1+2k^2$	k^2
nd	$1+k^2$	$2\quad k^2$	1
sc	$1\quad k^2$	$2\quad k^2$	1
cs	1	$2\quad k^2$	$1\quad k^2$
sd	$k^2(1\quad k^2)$	$1+2k^2$	1
ds	1	$1+2k^2$	$k^2(1\quad k^2)$
cd	k^2	$1\quad k^2$	1
dc	1	$1\quad k^2$	k^2

TABLE 1. Coe cients of equation (27) for each Jacobi elliptic function.

[4] K. CHANDRASEKHARAN, *Elliptic Functions*, Springer-Verlag, 1985, doi:10.1017/CBO9780511608759.

[5] C. CHENG AND G. KNORR, *The integration of the Vlasov equation in con guration space*, Journal of Computational Physics, 22 (1976), pp. 330 351, doi:https://doi.org/10.1016/0021-9991(76)90053-X, http://www.sciencedirect.com/science/article/pii/002199917690053X.

[6] N. CROUSEILLES AND M. LEMOU, *An asymptotic preserving scheme based on a micro-macro decomposition for collisional Vlasov equations: di usion and high- eld scaling limits.*, Kinetic and Related Models , 4 (2011), pp. 441 477, https://hal.archives-ouvertes.fr/hal-00533327.

[7] L. DEMEIO AND J. HOLLOWAY, *Numerical simulations of BGK modes*, Journal of Plasma Physics, 46 (1991), pp. 63 84, doi:10.1017/S0022377800015956.

[8] B. DESPR S, *Scattering structure and Landau damping for linearized Vlasov equations with inhomogeneous Boltzmannian states*, Ann. Henri Poincaré, 20 (2019), pp. 2767 2818.

[9] E. FAOU, R. HORSIN, AND F. ROUSSET, *On linear damping around inhomogeneous stationary states of the Vlasov-HMF model*, J. Dyn. Di . Equat., 33 (2020), pp. 1531 1577.

[10] F. FILBET, L. PARESCHI, AND T. REY, *On steady-state preserving spectral methods for homogeneous Boltzmann equations*, arXiv e-prints, (2014), arXiv:1408.1863, p. arXiv:1408.1863, arXiv:1408.1863.

[11] M. FONTAINE, *Mod les math matiques de type "Hamiltonian Mean-Field": stabilit et m thodes num riques autour d' tats stationnaires*, PhD thesis, ENS Rennes, 2018.

[12] A. GHIZZO, B. IZRAR, P. BERTRAND, E. FIJALKOW, M. R. FEIX, AND M. SHOUCRI, *Stability of Bernstein Greene Kruskal plasma equilibria. numerical experiments over a long time*, The Physics of Fluids, 31 (1988), pp. 72 82, doi:10.1063/1.866579, https://aip.scitation.org/doi/abs/10.1063/1.866579, arXiv:https://aip.scitation.org/doi/pdf/10.1063/1.866579.

[13] L. GOSSE AND G. TOSCANI, *Space localization and well-balanced schemes for discrete kinetic models in di usive regimes*, SIAM Journal on Numerical Analysis, 41 (2003), pp. 641 658, doi:10.1137/S0036142901399392, https://doi.org/10.1137/S0036142901399392.

[14] L. GOSSE AND G. TOSCANI, *Asymptotic-preserving and well-balanced schemes for radiative transfer and the rosseland approximation*, Numerische Mathematik, 98 (2004), pp. 223 250.

[15] Y. GUO AND Z. LIN, *The existence of stable BGK waves*, Communications in Mathematical Physics, 352 (2017), pp. 1121 1152, doi:10.1007/s00220-017-2873-2, https://doi.org/10.1007/s00220-017-2873-2.

[16] Y. GUO AND W. A. STRAUSS, *Instability of periodic BGK equilibria*, Communications on Pure and Applied Mathematics, 48 (1995), pp. 861 894, doi:10.1002/cpa.3160480803, https://onlinelibrary.wiley.com/doi/abs/10.1002/cpa.3160480803, arXiv:https://onlinelibrary.wiley.com/doi/pdf/10.1002/cpa.3160480803.

[17] S. JIN AND Y. SHI, *A micro-macro decomposition-based asymptotic-preserving scheme for the multispecies Boltzmann equation*, SIAM J. Scienti c Computing, 31 (2010), pp. 4580 4606, doi:10.1137/090756077.

[18] L. D. LANDAU, *On the vibrations of the electronic plasma*, J. Phys.(USSR), 10 (1946), pp. 25 34. [Zh. Eksp. Teor. Fiz.16,574(1946)].

[19] G. LATU, V. GRANDGIRARD, J. ABITEBOUL, N. CROUSEILLES, G. DIF-PRADALIER, X. GARBET, P. GHENDRIH, M. MEHRENBERGER, Y. SARAZIN, AND E. SONNENDR CKER, *Improving conservation properties in a 5D gyrokinetic semi-Lagrangian code*, European Journal of Physics D, 68 (2014), p. 345, doi:10.1140/epjd/e2014-50209-1, https://hal.inria.fr/hal-00966162.

[20] M. Lemou and L. Mieussens, *A new asymptotic preserving scheme based on micro-macro formulation for linear kinetic equations in the di usion limit*, SIAM J. Scienti c Computing, 31 (2008), pp. 334 368, doi:10.1137/07069479X.

[21] Z. Lin, *Instability of periodic BGK waves*, Mathematical Research Letters, 8 (2001), doi:10.4310/MRL.2001.v8.n4.a11.

[22] Z. Lin, *Nonlinear instability of periodic BGK waves for Vlasov-Poisson system*, Communications on Pure and Applied Mathematics, 58 (2005), pp. 505 528, doi:10.1002/cpa.20028, https://onlinelibrary.wiley.com/doi/abs/10.1002/cpa.20028, arXiv:https://onlinelibrary.wiley.com/doi/pdf/10.1002/cpa.20028.

[23] T.-P. Liu and S.-H. Yu, *Boltzmann equation: Micro-macro decompositions and positivity of shock pro les*, Communications in Mathematical Physics, 246 (2004), pp. 133 179, doi:10.1007/s00220-003-1030-2, https://doi.org/10.1007/s00220-003-1030-2.

[24] L. Marradi, B. Afeyan, M. Mehrenberger, N. Crouseilles, C. Steiner, and E. Sonnendr cker, *Vlasov on GPU*, ESAIM: Proceedings, 43 (2013), pp. p. 37 58, doi:10.1051/proc/201343003, https://hal.archives-ouvertes.fr/hal-00908498. 20 pages, 7 gures. ESAIM Proceedings 2013.

[25] L. Pareschi and T. Rey, *Residual equilibrium schemes for time dependent partial di erential equations*, arXiv e-prints, (2016), arXiv:1602.02711, p. arXiv:1602.02711, arXiv:1602.02711.

[26] J. R Danielson, F. Anderegg, and C. Driscoll, *Measurement of Landau damping and the evolution to a BGK equilibrium*, Physical review letters, 92 (2004), p. 245003, doi:10.1103/PhysRevLett.92.245003.

[27] W. A. Schwalm, *Lectures on Selected Topics in Mathematical Physics: Elliptic Functions and Elliptic Integrals*, 2053-2571, Morgan & Claypool Publishers, 2015, doi:10.1088/978-1-6817-4230-4, http://dx.doi.org/10.1088/978-1-6817-4230-4.

[28] E. Sonnendr cker, J. Roche, P. Bertrand, and A. Ghizzo, *The semi-lagrangian method for the numerical resolution of the Vlasov equation*, Journal of Computational Physics, 149 (1999), pp. 201 220, doi:https://doi.org/10.1006/jcph.1998.6148, http://www.sciencedirect.com/science/article/pii/S0021999198961484.

[29] E. T. Whittaker and G. N. Watson, *A Course of Modern Analysis*, Cambridge Mathematical Library, Cambridge University Press, 4 ed., 1952, doi:10.1017/CBO9780511608759.